

Part 2. Helmholtz Equation Least Squares (HELS) Methods

Formulation

A quick recap — the sound waves from a loudspeaker can be fully expressed by one of the following equations:

$$\hat{p}(r, \theta, \phi; \omega) = \sum_{n=0}^{\infty} \sum_{m=-n}^n [A_{mn} j_n(kr) + B_{mn} y_n(kr)] Y_n^m(\theta, \phi)$$

and

$$\hat{p}(r, \theta, \phi; \omega) = \sum_{n=0}^{\infty} \sum_{m=-n}^n [A_{mn} h_n^{(1)}(kr) + B_{mn} h_n^{(2)}(kr)] Y_n^m(\theta, \phi)$$

If we are only seeking for an approximation, we don't need an infinite number of terms. The directivity patterns of a loudspeaker at low frequencies are usually quite simple, and a few low orders spherical harmonics is often enough to give a close approximation. At higher frequencies, the directivity patterns can get much more complicated. In these cases, higher orders spherical harmonics, and therefore a larger number of expansion terms, are required.

The Helmholtz Equation Least Squares (HELS) methods [1, p.9] simplifies our task by not trying to solve for the weighting coefficients, A_{mn} and B_{mn} , of the expansion terms analytically. Instead, it uses the linear least squares (multiple linear regression) methods to look for the closest approximates. The reason Helmholtz equation is in the method name is because these spherical wave functions are solutions to the Helmholtz equation in the spherical coordinates system.

There is a major difference between Klippel's approach and the approach proposed in this report. Klippel scans the loudspeaker in two concentric cylindrical surfaces around it. The approach proposed here scans in a zone around the loudspeaker bounded by two concentric spherical surfaces.

For the time being, let us focus only on the second equation from above for our solution. If we approximate with spherical harmonics only to up degree N , the truncated equation becomes:

$$\hat{p}(r, \theta, \phi; \omega) = \sum_{n=0}^N \sum_{m=-n}^n [A_{mn} h_n^{(1)}(kr) + B_{mn} h_n^{(2)}(kr)] Y_n^m(\theta, \phi) \quad (2.1)$$

For $N = 1$, we can expand equation (2.1) to:

$$\begin{aligned} \hat{p}(r, \theta, \phi; \omega) = & \left[A_{0,0} h_0^{(1)}(kr) + B_{0,0} h_0^{(2)}(kr) \right] Y_0^0(\theta, \phi) \\ & + \left[A_{-1,1} h_1^{(1)}(kr) + B_{-1,1} h_1^{(2)}(kr) \right] Y_1^{-1}(\theta, \phi) \\ & + \left[A_{0,1} h_1^{(1)}(kr) + B_{0,1} h_1^{(2)}(kr) \right] Y_1^0(\theta, \phi) \\ & + \left[A_{1,1} h_1^{(1)}(kr) + B_{1,1} h_1^{(2)}(kr) \right] Y_1^1(\theta, \phi) \end{aligned} \quad (2.2)$$

We have a total of 4 spherical harmonics and 8 weighting coefficients in this $N = 1$ case. If we have sound pressure measurements made at 8 (or more) different locations, we can form 8 (or more) equations to solve for the 8 unknown weighting coefficients. Once the weighting coefficients are determined, we can back substitute them into equation (2.2), and we will have an equation that we can use to reconstruct the (approximated) sound pressure field anywhere in the 3D space. This is the basic idea of our method — obtain pressure measurement data at a number of different locations around a sound source, use the measurements to solve for the weighting coefficients, and use these weighting coefficients to reconstruct the sound pressure field anywhere in the entire 3D space. The reconstruction will not be exact as only a finite number of spherical wave expansion terms are used.

In general, if we model our problem with spherical harmonics to order N , we will have a total of $1 + 3 + 5 + \dots + (2N + 1) = (N + 1)^2$ spherical harmonics, and we will need to solve for $2(N + 1)^2$ weighting coefficients. It should be obvious that, for example if we chose $N = 10$, we will need a minimum of $2(10 + 1)^2 = 242$ measurement points. If we have fewer than 242 measurements, we will have a under-determined system and the weighting coefficients cannot be uniquely determined. In practice, we almost always want to provide more measurements than the number of weighting coefficients we need to solve for. (Klippel suggested a measurement points to coefficients ratio of 1.5 [2, slide 30].) This results in an over-determined system as we have more equations than unknowns. The standard solution method for over-determined systems is least squares.

Linear Least Squares

The type of least squares methods we use to solve for the weight coefficient is linear least squares. As linear least squares problems are best solved using linear algebra methods, we will start using matrix notations. Interested readers unfamiliar with numerical linear least squares methods may want to read Cleve Moler's Numerical Computing with MATLAB, Chapter 5, Least Squares, and possibly Chapter 10, Eigenvalues and Singular Values [3] (free download). (For readers unfamiliar with linear algebra but are interested in gaining a college level proficiency on the subject, the video lectures in the MIT OpenCourseWare linear algebra class by professor Gilbert Strang [4] is an excellent resource.)

For $N = 1$ and with H measurements, we rewrite equation (2.2) in matrix form below. Due to page width restriction, only column 1 for the spherical wave expansion terms matrix is written in full. It is understood that for the abbreviated columns, the arguments for the spherical Hankel functions and spherical harmonics are the same as column 1.

$$\begin{bmatrix} \hat{p}(r_1, \theta_1, \phi_1; \omega) \\ \hat{p}(r_2, \theta_2, \phi_2; \omega) \\ \vdots \\ \hat{p}(r_H, \theta_H, \phi_H; \omega) \end{bmatrix} = \begin{bmatrix} h_0^{(1)}(kr_1)Y_0^0(\theta_1, \phi_1) & h_0^{(2)}Y_0^0 & h_1^{(1)}Y_1^{-1} & h_1^{(2)}Y_1^{-1} & h_1^{(1)}Y_1^0 & h_1^{(2)}Y_1^0 & h_1^{(1)}Y_1^1 & h_1^{(2)}Y_1^1 \\ h_0^{(1)}(kr_2)Y_0^0(\theta_2, \phi_2) & h_0^{(2)}Y_0^0 & h_1^{(1)}Y_1^{-1} & h_1^{(2)}Y_1^{-1} & h_1^{(1)}Y_1^0 & h_1^{(2)}Y_1^0 & h_1^{(1)}Y_1^1 & h_1^{(2)}Y_1^1 \\ \vdots & \vdots & \vdots & \vdots & \vdots & \vdots & \vdots & \vdots \\ h_0^{(1)}(kr_H)Y_0^0(\theta_H, \phi_H) & h_0^{(2)}Y_0^0 & h_1^{(1)}Y_1^{-1} & h_1^{(2)}Y_1^{-1} & h_1^{(1)}Y_1^0 & h_1^{(2)}Y_1^0 & h_1^{(1)}Y_1^1 & h_1^{(2)}Y_1^1 \end{bmatrix} \begin{bmatrix} A_{0,0} \\ B_{0,0} \\ A_{-1,1} \\ B_{-1,1} \\ A_{0,1} \\ B_{0,1} \\ A_{1,1} \\ B_{1,1} \end{bmatrix} \quad (2.3)$$

We can shorten the equation to:

$$[\hat{p}]_{H \times 1} = [\Psi]_{H \times M} [c]_{M \times 1} \quad (2.4)$$

where H is number of measurements, and
 M is the number of weighting coefficients, with $M = 2(N + 1)^2$

$[\hat{p}]$ is a column vector of length H ; $[\Psi]$ is a matrix of H rows by M columns; and $[c]$ is a column vector of length M .

The function `numpy.linalg.lstsq()` from the Python Numpy library is the solver used in the examples in this report. The `lstsq()` function utilizes singular value decomposition (SVD) to solve for vector $[c]$ when given matrix $[\Psi]$ and vector $[\hat{p}]$. In addition to our desired solution $[c]$, the `lstsq()` function also returns the least squares *residuals*, the *rank* of $[\Psi]$, and its *singular values*. These additionally returned values are very useful for assessing the quality of the least squares solutions.

The *residuals* indicates how close our fit is to the data. However, it is not a totally reliable indicator. Sometimes we may overfit. It is usually a good practice to set aside a portion of the measurement data, not use them in the least squares calculations, but use them to calculate the reconstruction errors. This is a much more robust method to assess the quality of our fit. It is similar to machine learning where we divide our data into a training set and a test set.

The *rank* of matrix $[\Psi]$ should be equal to its number of columns M (which is the same as the number of weighting coefficients). If the rank is lower, $[\Psi]$ is *rank deficient*, which means that the columns of $[\Psi]$ are not independent and we cannot determine the weighting coefficients uniquely. The *singular values* can tell us if our matrix is well-conditioned or ill-conditioned. The singular values returned by `lstsq()` are ordered with the largest being first and the smallest being last. The *condition number* is ratio between the largest and smallest singular values. A large condition number means that our matrix system is close to being singular (rank deficient), and it is an indication that our problem is mathematically *ill posed* and our solution is likely to be of poor accuracy and, therefore, unreliable.

When we have determined $[c]$, we can proceed to reconstruct the pressure field using using equation(2.5). The matrix $[\Psi^{recon}]$ is formed by using the coordinates of the reconstruction points.

$$[\hat{p}^{recon}]_{K \times 1} = [\Psi^{recon}]_{K \times M} [c]_{M \times 1} \quad (2.5)$$

where K is number of reconstruction points

One Way to Get a Rank Deficient System

Let's see what happens if we decided to perform all our measurements on a spherical surface centered to the origin of the spherical coordinate system. This means all our measurements are taken with the same radial coordinate r_s . We substitute our measurement points coordinates into equation (2.3). For brevity, only the first two columns of $[\Psi]$ are shown:

$$\begin{aligned}
\begin{bmatrix} \hat{p}(r_s, \theta_1, \phi_1; \omega) \\ \hat{p}(r_s, \theta_2, \phi_2; \omega) \\ \vdots \\ \hat{p}(r_s, \theta_H, \phi_H; \omega) \end{bmatrix} &= \begin{bmatrix} h_0^{(1)}(kr_s)Y_0^0(\theta_1, \phi_1) & h_0^{(2)}(kr_s)Y_0^0(\theta_1, \phi_1) & \dots \\ h_0^{(1)}(kr_s)Y_0^0(\theta_2, \phi_2) & h_0^{(2)}(kr_s)Y_0^0(\theta_2, \phi_2) & \dots \\ \vdots & \vdots & \vdots \\ h_0^{(1)}(kr_s)Y_0^0(\theta_H, \phi_H) & h_0^{(2)}(kr_s)Y_0^0(\theta_H, \phi_H) & \dots \end{bmatrix} \begin{bmatrix} A_{0,0} \\ B_{0,0} \\ A_{-1,1} \\ B_{-1,1} \\ A_{0,1} \\ B_{0,1} \\ A_{1,1} \\ B_{1,1} \end{bmatrix} \\
&= \begin{bmatrix} c_1 Y_0^0(\theta_1, \phi_1) & c_2 Y_0^0(\theta_1, \phi_1) & \dots \\ c_1 Y_0^0(\theta_2, \phi_2) & c_2 Y_0^0(\theta_2, \phi_2) & \dots \\ \vdots & \vdots & \vdots \\ c_1 Y_0^0(\theta_H, \phi_H) & c_2 Y_0^0(\theta_H, \phi_H) & \dots \end{bmatrix} \begin{bmatrix} A_{0,0} \\ B_{0,0} \\ A_{-1,1} \\ B_{-1,1} \\ A_{0,1} \\ B_{0,1} \\ A_{1,1} \\ B_{1,1} \end{bmatrix}
\end{aligned}$$

By replacing $h_0^{(1)}(kr_s)$ with c_1 and $h_0^{(2)}(kr_s)$ with c_2 it can be seen that columns 1 and 2 are multiples of each other. The same applies for columns 3 and 4 and so on. With this matrix $[\Psi]$, we will not be able to separately determine $A_{0,0}$ and $B_{0,0}$, $A_{-1,1}$ and $B_{-1,1}$, and so on. The rank of $[\Psi]$ is only 4 and it has 8 columns. $[\Psi]$ is rank deficient.

`lstsq()` can still return useful solutions that can be used to recreate the acoustic pressure field. However, without being able to uniquely solve for the values of the coefficients A_{mn} and B_{mn} , we lack knowledge of the pressure field in the radial direction. The values of A_{mn} and B_{mn} returned by `lstsq()` are somewhat arbitrary as the solution is not unique. Since we don't know the proper values of A_{mn} , which are the weighting coefficients for the Hankel functions of the first kind $h_n^{(1)}(kr)$, and B_{mn} , which are the weighting coefficients for the Hankel functions of the second kind $h_n^{(2)}(kr)$, we will not be able to separate the outgoing waves from the incoming waves. In this situation, we will be unable to perform sound field separation.

If you think about it, it is intuitive that if we want to get information about the traveling direction of a wave, we need to take measurements at locations that are at different distances from the source. Therefore, we need to take our sound pressure measurements at different distances from the loudspeaker. In the simulations in this report, the angular coordinates of the measurement points are placed in a grid with uniform angular spacing, and the radial coordinates are randomly distributed between an outer and an inner limits (i.e. between two concentric spherical surfaces centered to the origin of the coordinate system).

Simulations

Generating Simulated Inputs

At this point we are ready to begin experimenting with numerical simulations. But first we need to be able to generate our simulated measurement data. To mimic closely how

a loudspeaker will be tested, we can mathematically create a few point sources that produce a chirp or an impulse signal. We generate a measurement grid, and simulate the sound pressures $p(r, \theta, \phi; t)$ as received at each grid point. We then Fourier transform the time measurements into complex pressure amplitudes, select a target frequency, extract the complex pressure amplitude at that frequency, and we have our simulated sound pressure amplitudes $\hat{p}(r, \theta, \phi; \omega)$.

This takes, however, quite a bit of computations. Quicker results from a more efficient method would be nice.

An outward traveling wave created by a *unit impulse* at the origin in free space is given by:

$$p(x, t) = \frac{1}{x} \delta(t - \frac{x}{c}) \quad (2.6)$$

where t is time, and
 x is the distance from the source

The amplitude of the wave is inversely proportional to its distance from the source — when the distance doubles, the amplitude is halved. As dB SPL is $20 \log_{10}(p/p_{ref})$, we can see that we are following the usual 6 dB SPL reduction with every doubling of distance in free space (inverse square law).

Apply Fourier transform to equation (2.6):

$$\begin{aligned} \hat{p}(x, \omega) &= \frac{1}{x} e^{i \frac{x}{c} \omega} \\ &= \frac{1}{x} e^{ikx} \end{aligned} \quad (2.7)$$

There we go! For each measurement point, simply calculate the distance from each point source and apply equation (2.7), and scale to the strength of the source. We then sum the pressure amplitudes from all point sources as Fourier transforms are linear, and we have our simulated pressure amplitudes.

Visualizing Sound Radiation Patterns

Figure 1 shows the directivity balloon plots of the simulated sound sources at various frequencies. The plots show the magnitudes of the sound pressures on the spherical surface 1 m from the origin. The radial distances of the balloon surfaces from the origin are the magnitudes of simulated sound pressure amplitudes (remember that the amplitudes are complex numbers) at the 1 m radius sphere. Only a half-section is plotted to give the sectioned view. In these simulations, the radiation pattern is symmetric to the cut plane.

Very fine angular spacing of 1° are used to generate these plots. The coordinates of the simulated sources are $(0, 0.1, 0.1)$, $(0, 0.1, -0.1)$, $(0, -0.1, 0.1)$ and $(0, -0.1, -0.1)$, and they are displayed as magenta 3D crosses. Distances are in meters. The 4 sources have equal strengths at 0.25 arbitrary units each.

At the low frequency of 100 Hz, the 4 sources essentially combined into one monopole. The diagonal (furthest) distances between the sources are $\sqrt{0.2^2 + 0.2^2} = 0.28$ m, and is the wavelength of a 1217 Hz sound wave. The combined source starts to noticeably deviate from

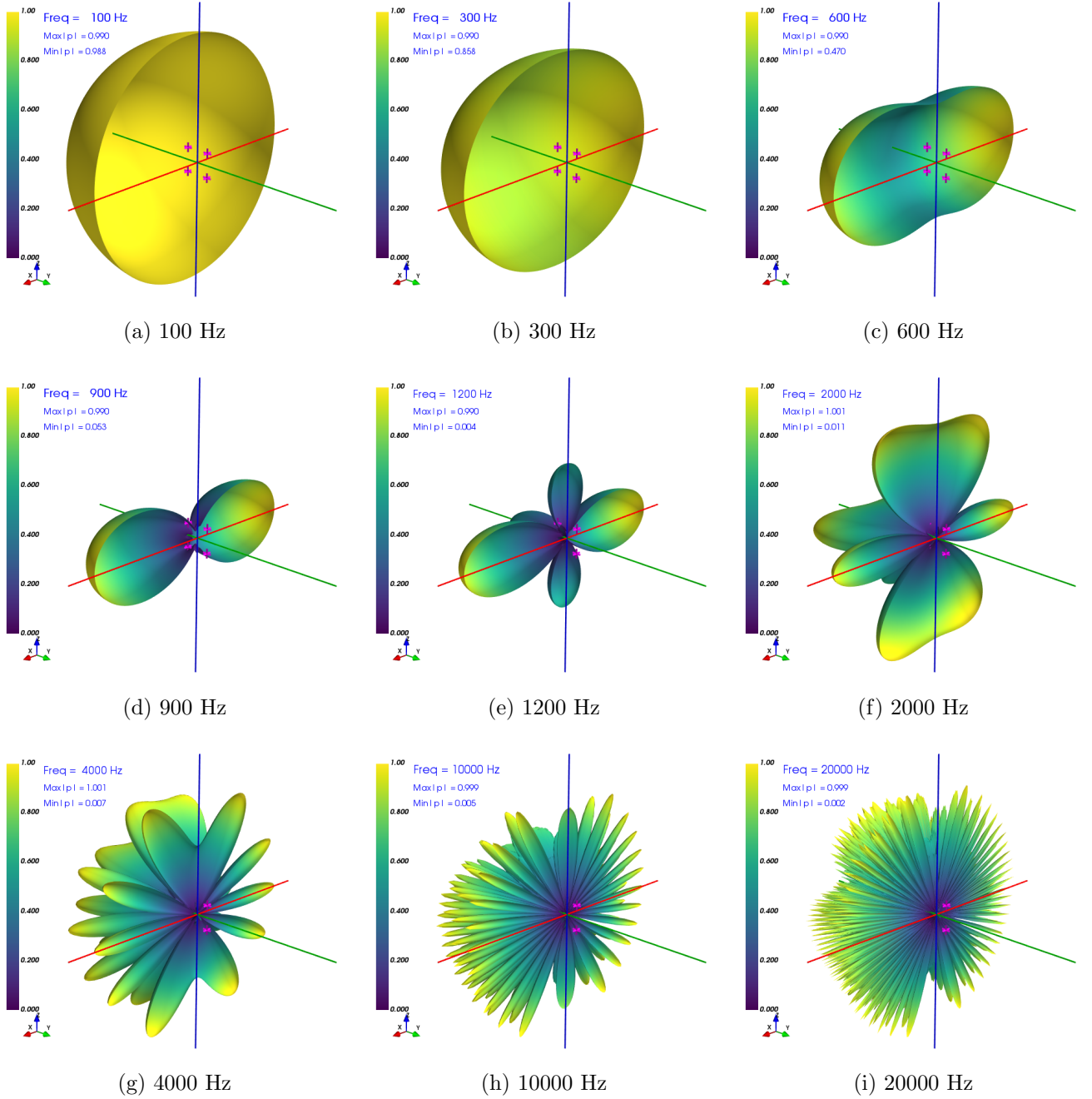


Figure 1: Directivity Patterns of the Simulated Sound Source at Various Frequencies

a monopole at around $0.25 \times$ this frequency (approx. 300 Hz). At about 900 Hz, its radiation pattern becomes similar to that of a dipole. The lateral distance between the point sources is 0.2 m and is equivalent to the wavelength of 1715 Hz. The two pairs of sources cancel each other (by destructive interference) in the y and z axes directions as their distance of separation is close to half the sound wave wavelength, which means they are close to 180° out-of-phase.

Above 900 Hz, more lobes start forming, and the directivity pattern becomes more and more complicated as frequency increases. At 20000 Hz, there are so many lobes that even plotting using 1° angular spacing is not sufficient to adequately resolve them.

Most loudspeakers aim to have only one driver active at a time at a mid to high frequency. (A notable exception is of course the troublesome cross-over regions.) This reduces the directivity complexity. Those with multiple drivers generating sound simultaneously, such as line arrays, have complicated directivity patterns. They will require high order spherical wave expansion functions to approximate and thus necessitate a large number of measurement points to characterize.

The Measurement Grid

Figure 2 shows the measurement grid used in the simulations. The grid spacing for both θ and ϕ are 7.5° , giving 1106 total points. The values for r are randomly distributed between 0.95 and 1.05 m. For reference, a shaded half sphere with 1 m radius centered to the origin is included in the figure. The magenta crosses near the center shows 4 simulated points sources. The 4 sources have equal output strengths at 0.25 arbitrary units each.

1106 Points

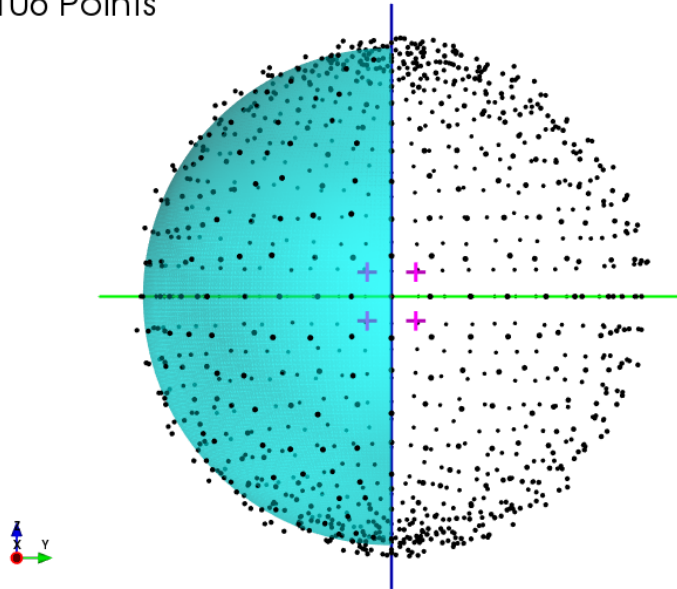


Figure 2: Simulated Measurement Grid — 1106 Points

This measurement grid is sub-optimal as more measurement points are concentrated near the north and south poles, while they are more sparse near the equator. This is opposite to what we normally desire. Optimization of the measurement grid, however, is not pursued in this report and is left as an item for future improvement.

Sound Pressure Field Reconstruction

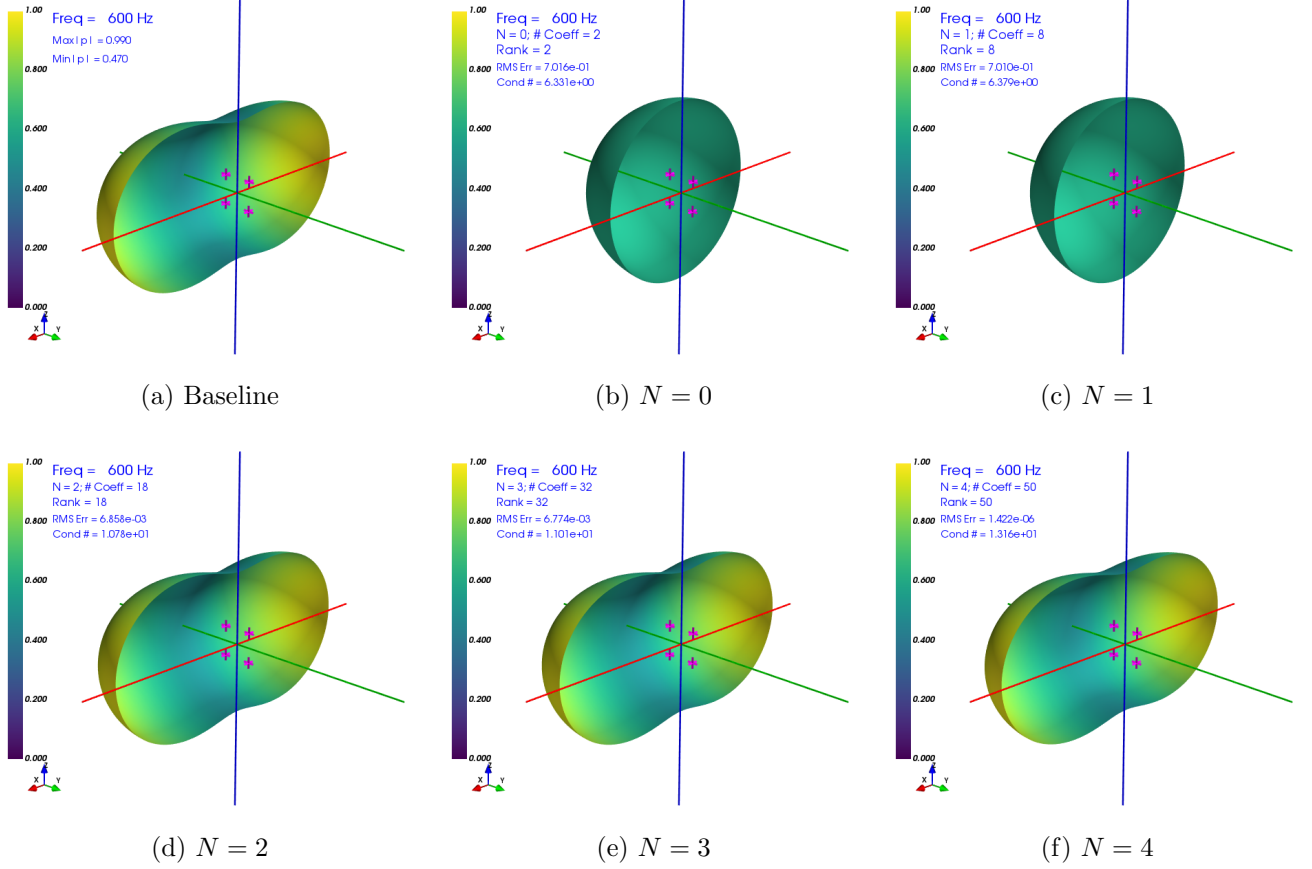


Figure 3: Sound Pressure Field Reconstruction at 600 Hz

Figure 3 shows the pressure field reconstruction at 600 Hz with N from 0 to 4. Figure 3(a) is the baseline, which is a copy of the 600 Hz plot from Figure 1. At 600 Hz, the directivity pattern is very simple. If we are targeting reconstruction RMS error < 0.01 (-40 dB) calculated using the residuals returned by the least squares solver, we can achieve satisfactory reconstruction with $N = 2$. Note that the much more robust method of error estimation is to compare the reconstructions to a separate test data set. However, since we are also verifying the reconstruction quality by visually comparing the 3D plots, we will not be estimating errors using a test data set in this report.

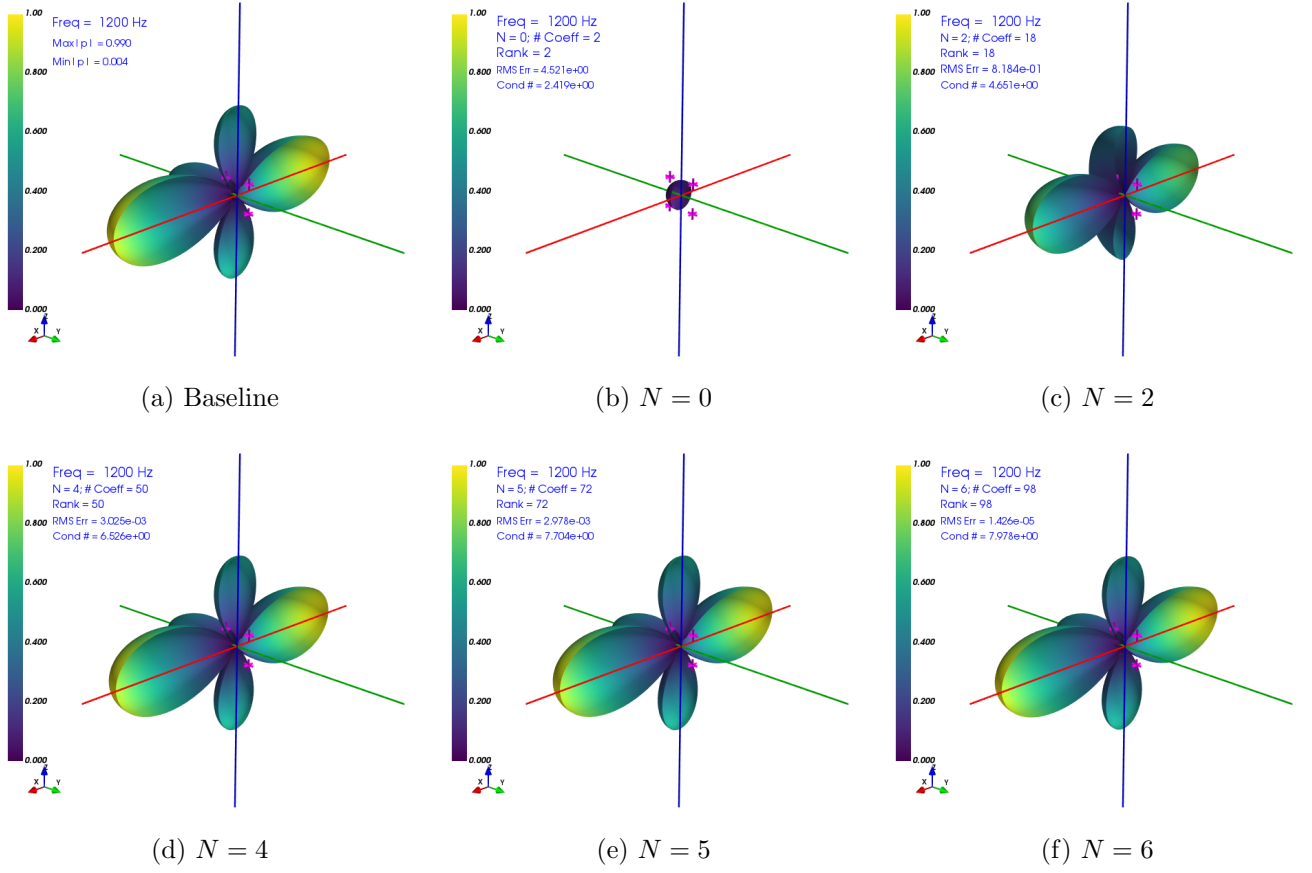


Figure 4: Sound Pressure Field Reconstruction at 1200 Hz

Figure 4 shows the reconstruction at 1200 Hz. Satisfactory reconstruction is reached with $N = 4$.

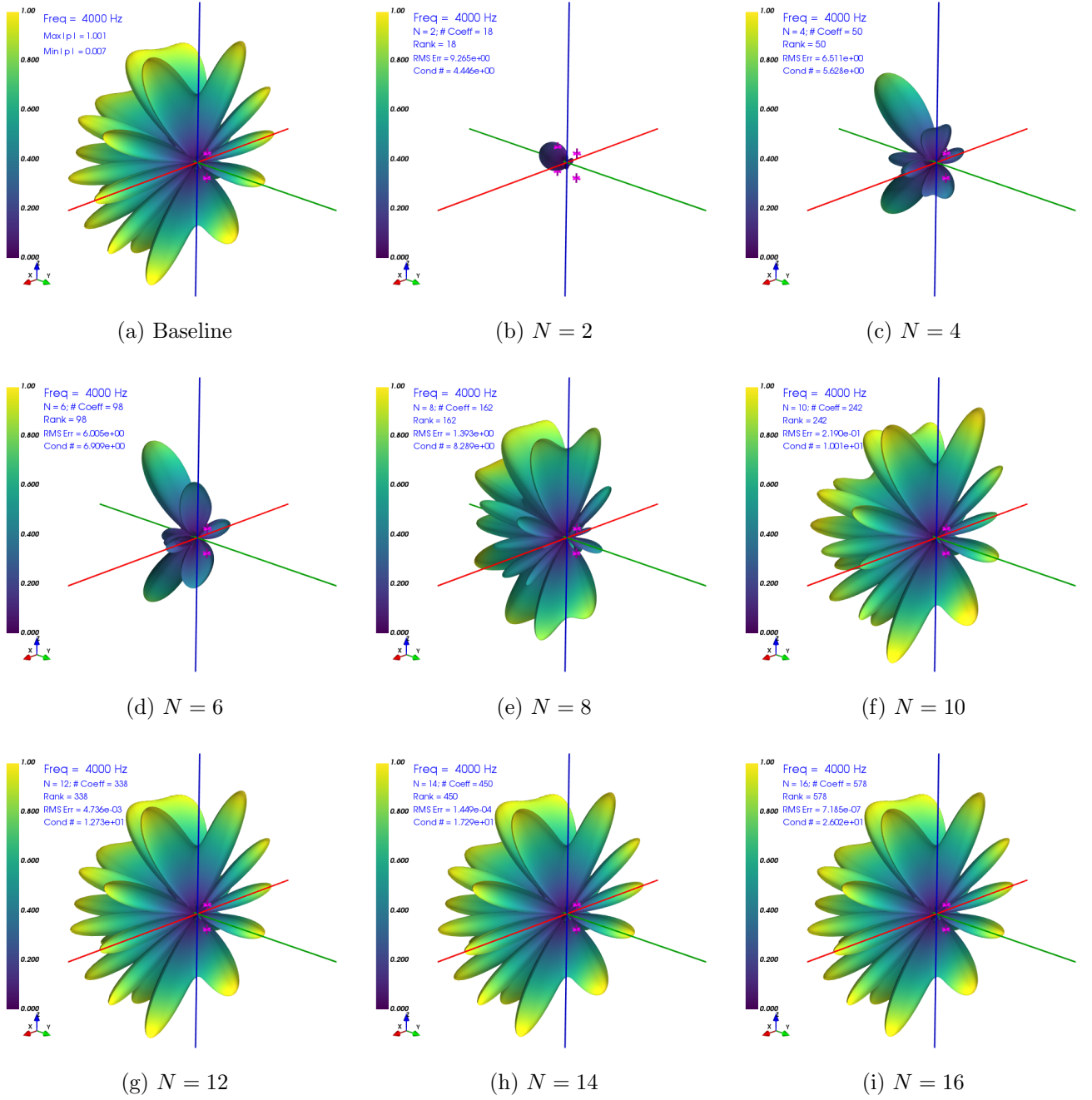


Figure 5: Sound Pressure Field Reconstruction at 4000 Hz

Figure 5 shows the reconstruction at 4000 Hz. Satisfactory reconstruction is reached with $N = 12$.

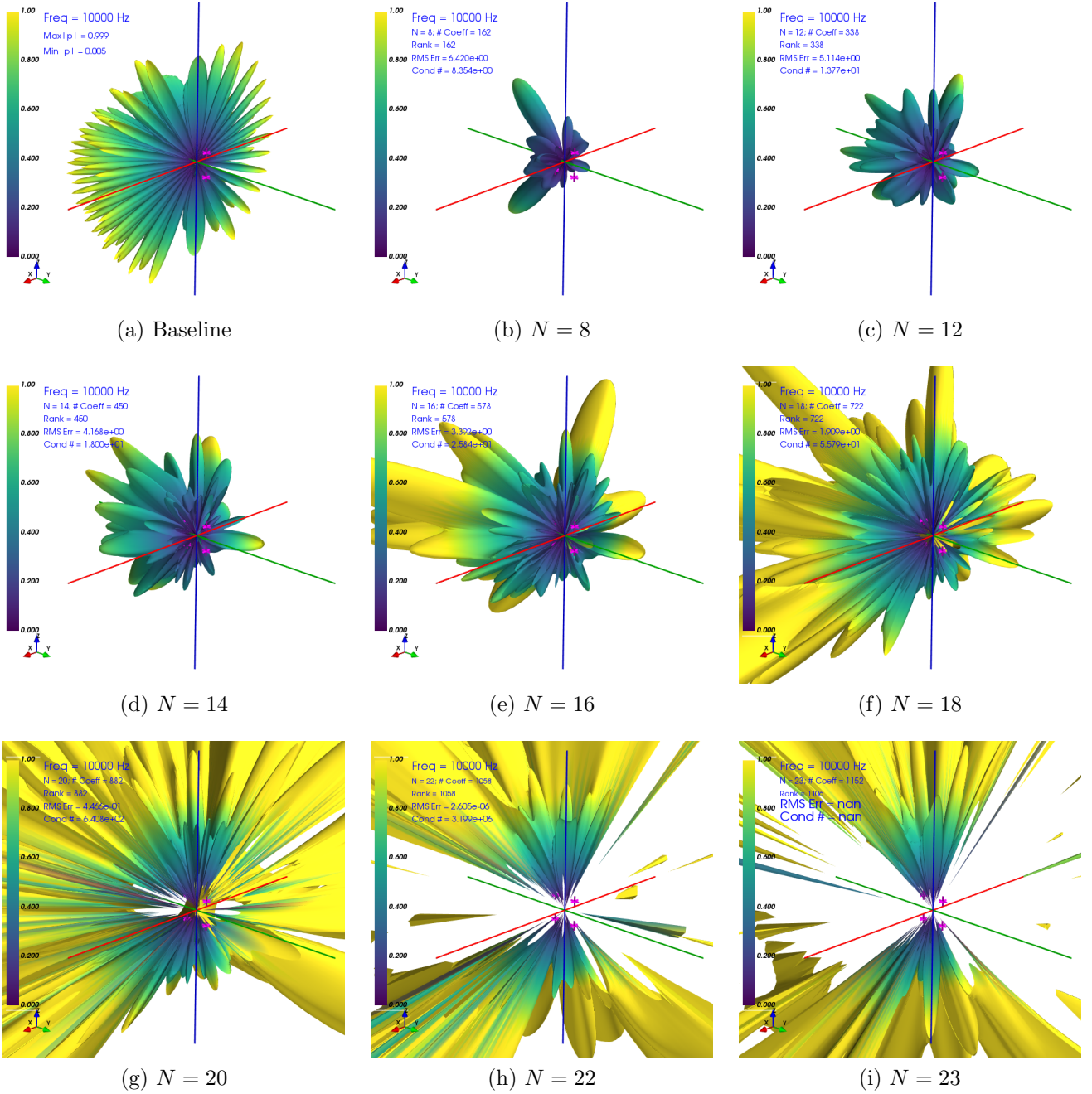


Figure 6: Sound Pressure Field Reconstruction at 10000 Hz

Figure 6 shows the reconstruction at 10000 Hz. It is clear that we failed to find a satisfactory solution. At $N = 22$, even though the reported RMS error seems to suggest we have reached a solution, it is clearly incorrect. When $N \geq 23$, the number of coefficients we are solving for exceeds the number of measurement points, the problem becomes under-determined. The number of measurement points are insufficient to reconstruct this highly complex radiation pattern.

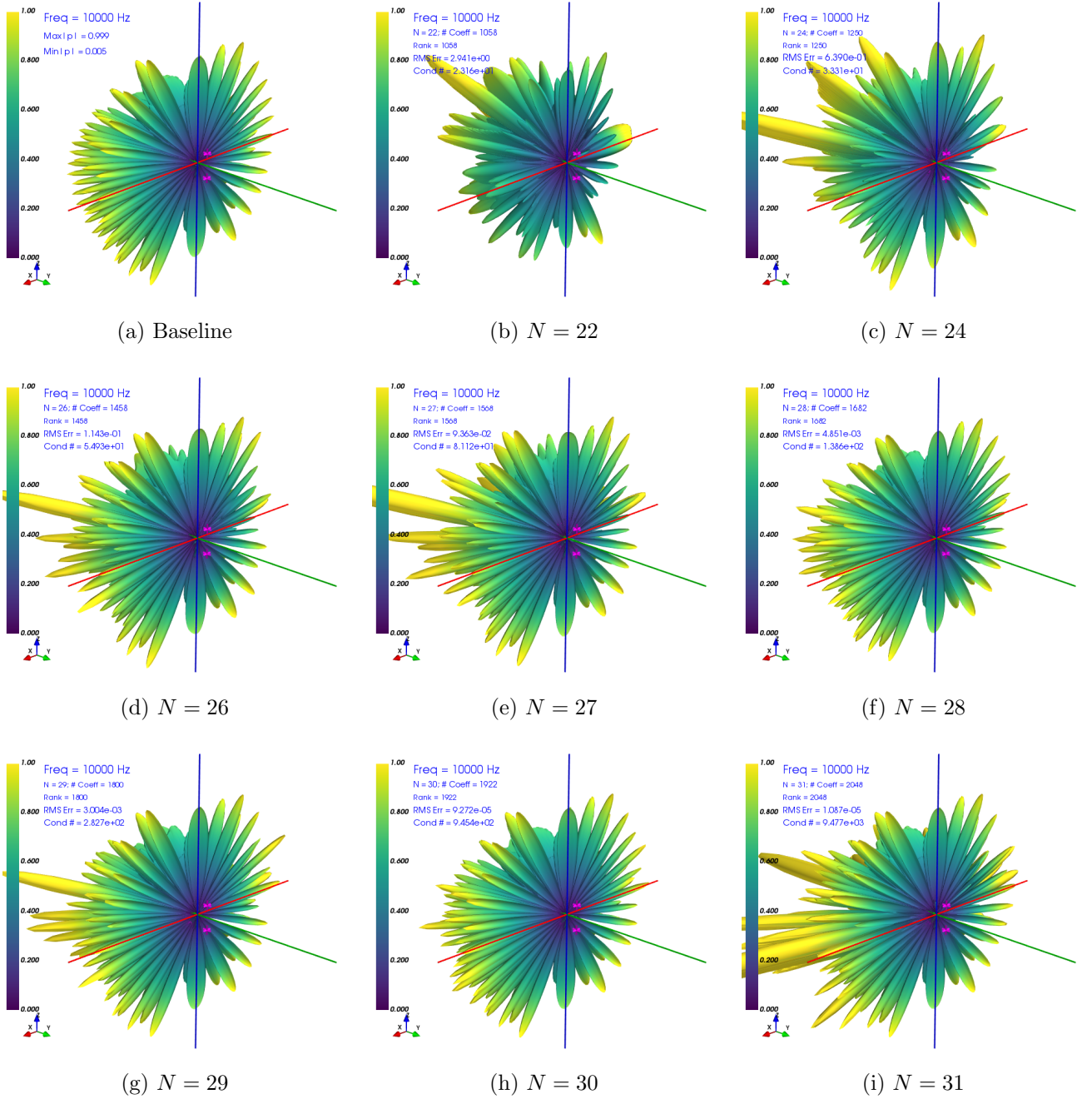


Figure 7: Reconstruction at 10000 Hz with 2522 Measurement Points

The measurement grid is made finer for the 10000 Hz reconstruction. The angular spacing is reduced from 7.5° to 5° , and the number of measurement points is increased from 1106 to 2522. Figure 7 shows the reconstructions. We barely managed to get a satisfactory approximation at $N = 28$. However, the solutions returned are unstable and oscillating. At $N = 29$, the approximation looks worse visually but the RMS error calculated using the residuals suggests otherwise. Still more measurement points are needed. Thankfully most

loudspeakers do not (and should not) have such complicated directivity patterns.

If we take our loudspeaker measurements in an anechoic chamber, we now have a method to recreate the complete 3D sound pressure field. We simply enter the required coordinates per [ANSI/CTA-2034](#), reconstruct the sound pressures at the required frequencies, and generate the spinorama graphs.

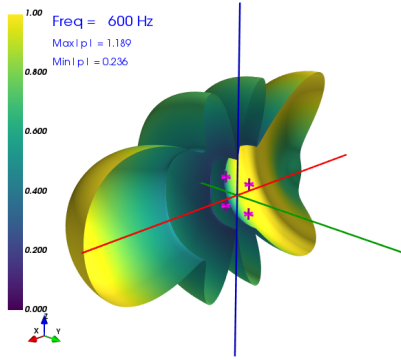
Sources Exterior to the Measurement Zone

The sources in the previous simulations are all inside of the measurement zone. In a non-anechoic space, we will have reflections from the room boundaries which will behave as sources from outside the measurement zone. We will use a simple model to test how well our method can handle such situations.

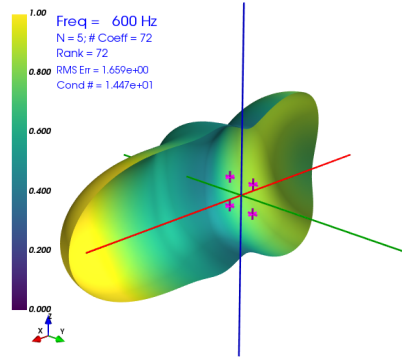
One inherent disadvantage of the HELS method is that it is based in the spherical coordinate system. The sound source is modeled with spherical expansion waves. If the sound source has a high aspect ratio, the accuracy of the approximation is reduced. We will see how well our method can reconstruct the sound pressure field from point sources that are placed both inside and outside the measurement zone. These simulated point sources combined together into a high aspect ratio sound source.

Figure 8 shows the reconstruction at 600 Hz. A duplicate set of the same 4 point sources is added outside the measurement zone at $x = -4$ m. This simulates a perfectly reflective wall at the plane $x = -2$ m. The 3D crosses representing the outside sources are outside the view and are not visible in the figures.

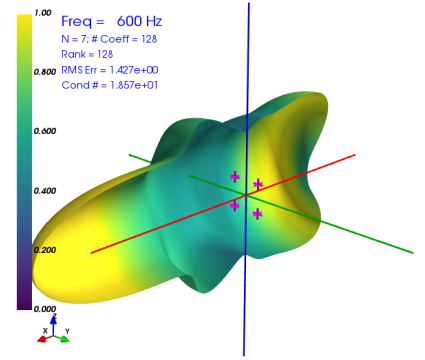
With sound sources spaced far apart, the sound pressure field pattern is significantly more complicated even at low frequencies. From the RMS error estimates, satisfactory reconstruction was achieved with $N = 13$. However, when looking at the directivity pattern plots, there are still noticeable differences between the reconstruction and the baseline. The previous simulation without the outside sources required only $N = 2$ to approximate at 600 Hz.



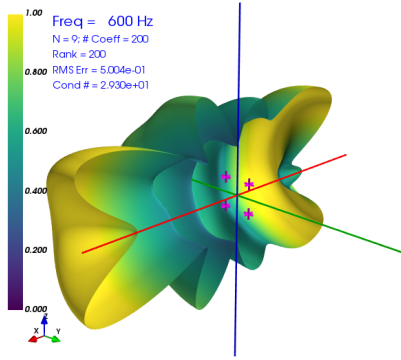
(a) Baseline



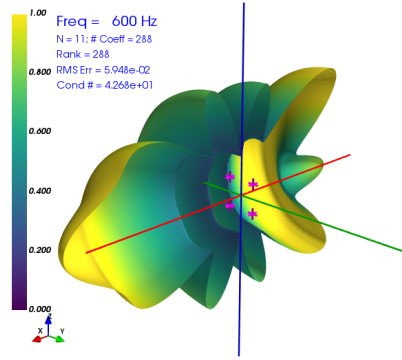
(b) $N = 5$



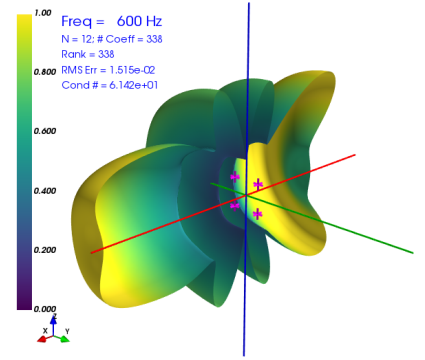
(c) $N = 7$



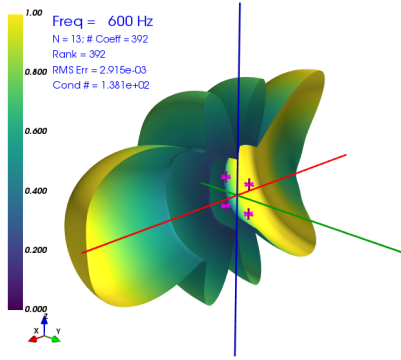
(d) $N = 9$



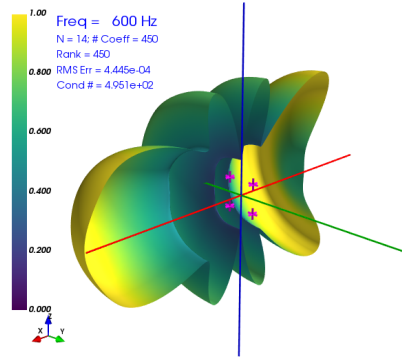
(e) $N = 11$



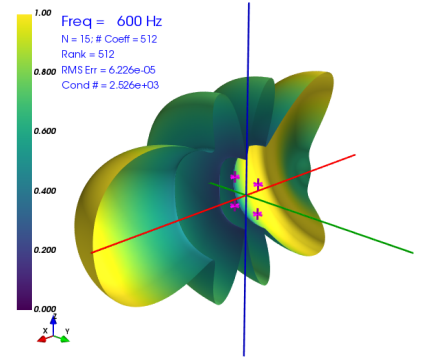
(f) $N = 12$



(g) $N = 13$



(h) $N = 14$



(i) $N = 15$

Figure 8: 600 Hz Reconstruction with Interior and Exterior Sources

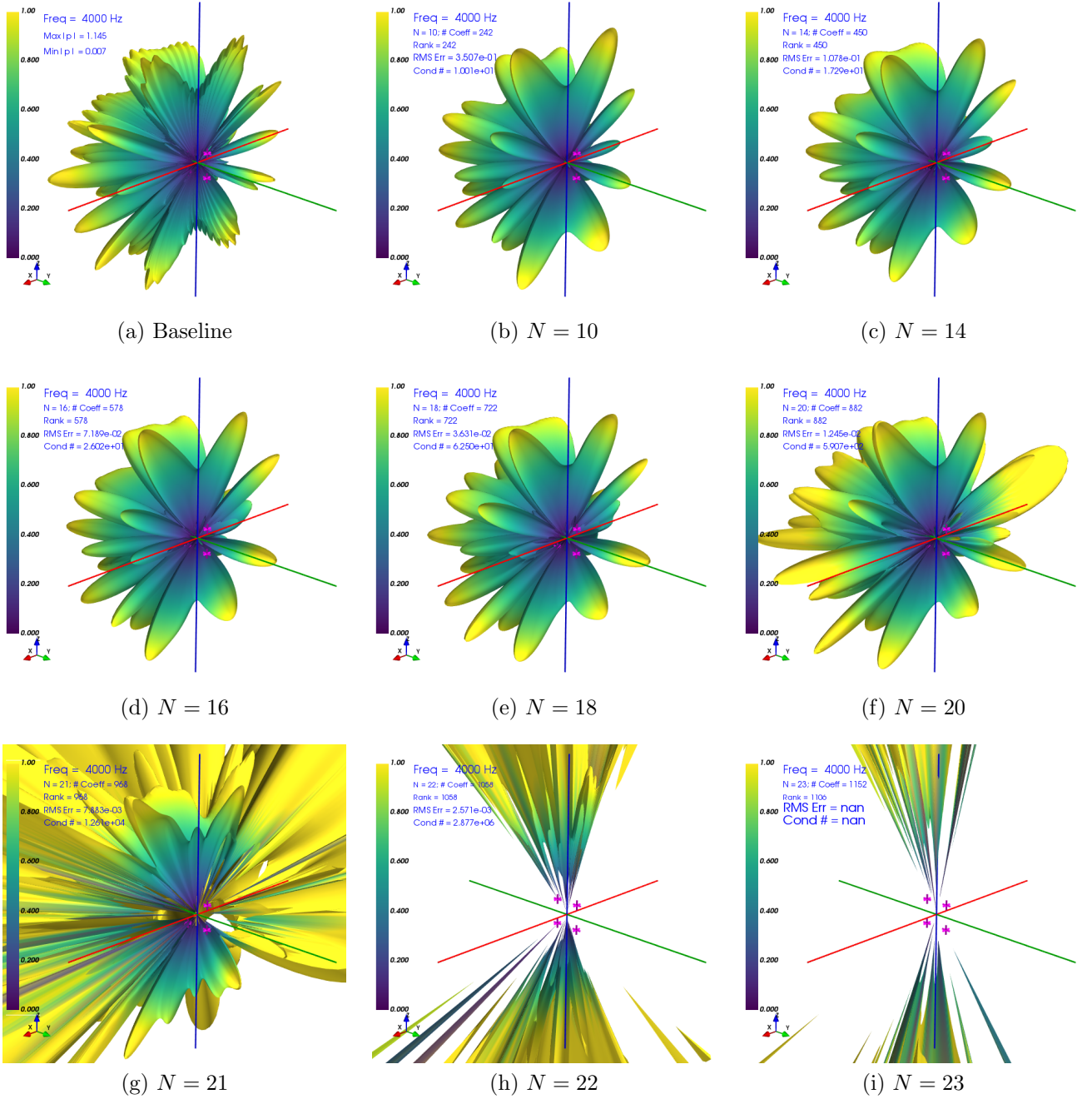


Figure 9: 4000 Hz Reconstruction with Interior and Exterior Sources

Figure 9 shows the reconstruction at 4000 Hz. The basic shape was reconstructed at about $N = 10$. No satisfactory solution was obtained. From the RMS error estimate, satisfactory reconstruction was supposedly achieved with $N = 21$, which was clearly incorrect. Solution diverged after $N \approx 18$. The 1106 measurements were insufficient to resolve the complex ripple patterns caused by the outside (reflected) sources.

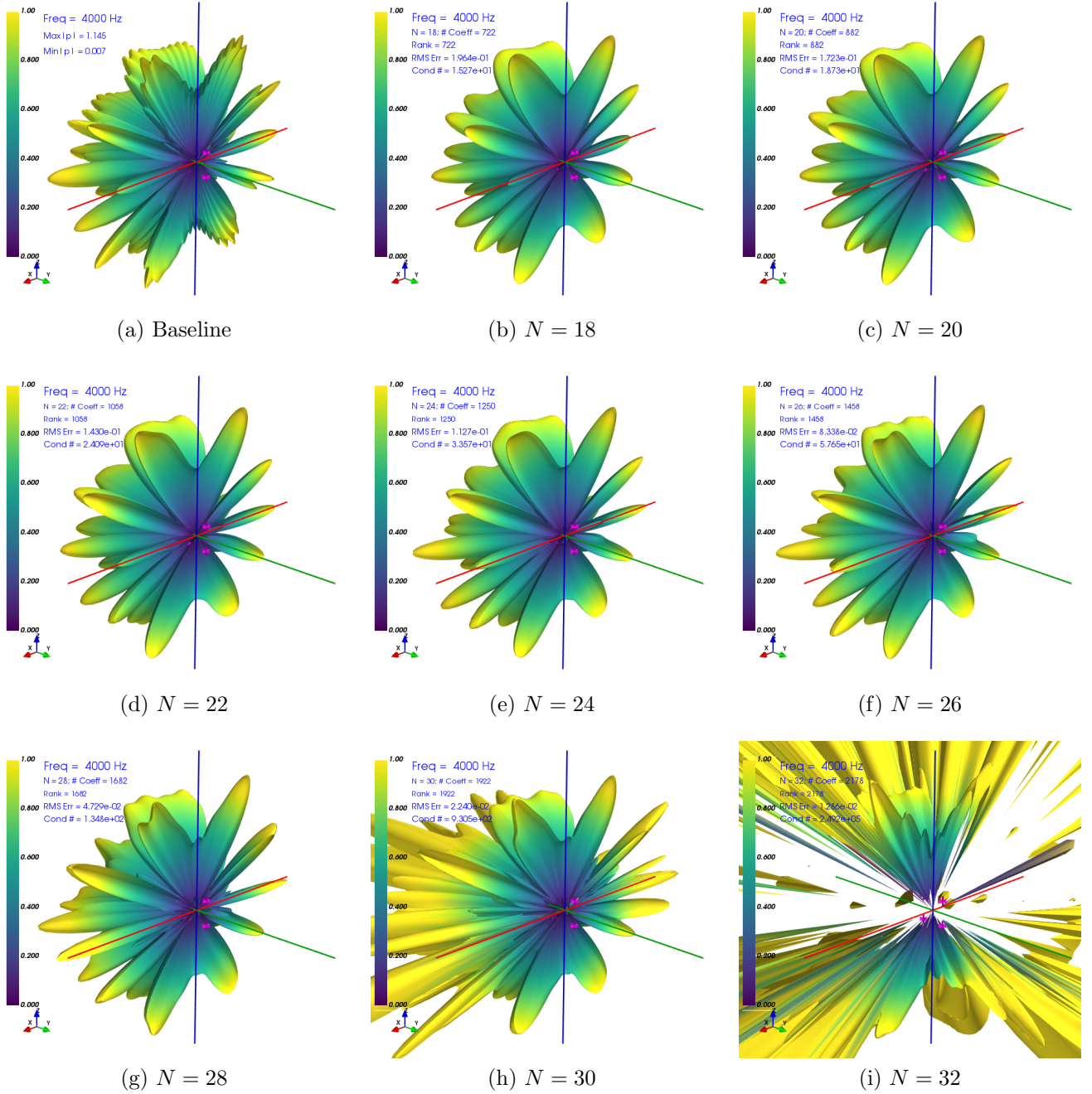


Figure 10: 4000 Hz Reconstruction with Interior and Exterior Sources, 5° Grid Spacing

Figure 10 shows the reconstruction at 4000 Hz with the 5° angular grid and 2522 measurement points. There is improvement over the 1106 points case. Ripples begin to appear at around $N \approx 26$. Estimated RMS Error was still above 0.01 at $N = 30$ when the solution started diverging.

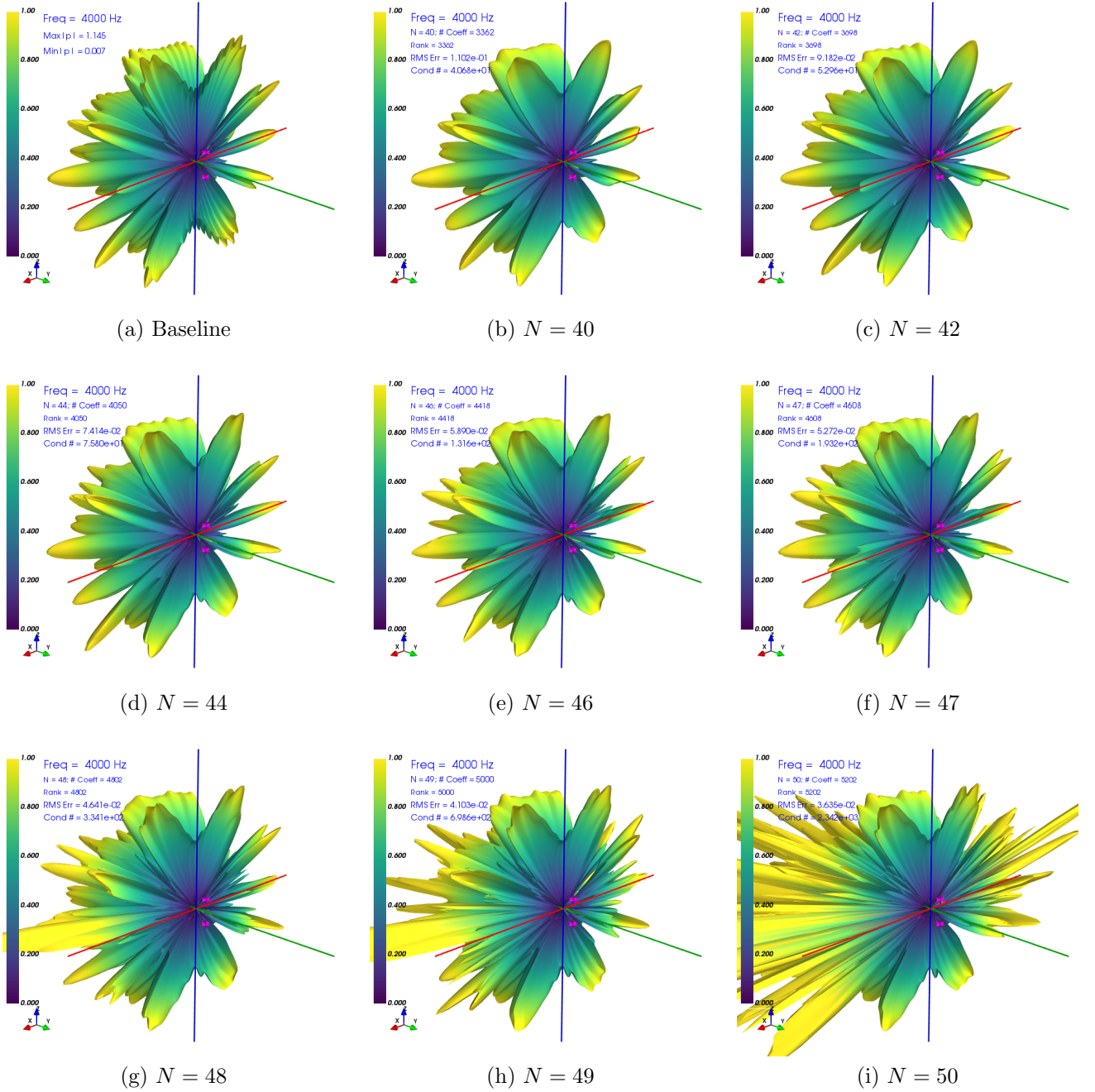


Figure 11: 4000 Hz Reconstruction with Interior and Exterior Sources, 3° Grid Spacing

Even with a super fine measurement grid of 3° angular grid spacing and 7082 measurement points, we are unable to meet our error target before our solution becomes unstable. Figure 11 shows the reconstructions. At this point, we will have to concede that we must either relax our error criteria or seek other methods.

In Klippel's Holographic Loudspeaker Testing poster [5, Section: Sound Separation], it is recommended, for frequencies above about 2800 Hz, when a lower frequency resolution is

not as much an issue, time windowed method be used for the measurements. The quasi-anechoic measurements at the higher frequencies eliminate the difficulties of reconstructing the very complicated pressure field patterns when strong room reflections are present. This also makes it unnecessary to apply sound field separation to remove the influences from the room reflections.

Klippel also used -20 dB as error criteria in the publication, A New Approach to Loudspeaker Measurements [6, Figure 3.0], instead of the -40 dB used in the simulations presented here. Real life measurements are imperfect. For example, errors in both sound pressure measurements and microphone positioning, and changes in the test environment such as fluctuations in the ambient noise during the scan, lower the data quality. All these result in a limit to the ultimate accuracy of our reconstruction.

In the publication Fast Loudspeaker Measurement in Non-Anechoic Environment [7, p.3, Section 3.2], Klippel reported that using their Near Field Scanner system for simple loudspeakers at low frequencies of < 1000 Hz, satisfactory results could be obtained with $N < 10$ and $100 - 200$ measurement points. For more complex line arrays and at higher frequencies of > 10000 Hz, $N > 30$ and > 3000 points may be required. Our simulation results seem to be consistent with those from Klippel's experience.

References

- [1] S. F. Wu, The Helmholtz Equation Least Squares Method, Springer Science+Business Media New York 2015
- [2] Klippel, Warkwyn, Holographic Measurement of the 3D Sound Field using Near-Field Scanning, 2015, Klippel GmbH, Dresden 01309, Germany
- [3] C. Moler, Numerical Computing with MATLAB, 2004, MathWorks
- [4] MIT OCW 18.06 Linear Algebra
- [5] Holographic Loudspeaker Testing Poster, Klippel GmbH, Dresden 01309, Germany
- [6] Dave Login, A New Approach to Loudspeaker Measurements, 2015, Klippel GmbH, Dresden 01309, Germany
- [7] C. Bellmann, W. Klippel, Fast Loudspeaker Measurement in Non-Anechoic Environment, Klippel GmbH, Dresden 01309, Germany